3D Band-Absorptive Frequency Selective Rasorber: Concept and Analysis

YUFENG YU[1], (Member, IEEE), **GUO QING LUO**[1], (Member, IEEE), **QI LIU**[2],
WEILIANG YU[1], **HUAYAN JIN**[1], **ZHEN LIAO**[1], **AND ZHONGXIANG SHEN**[3], (Fellow, IEEE)

[1]Key Laboratory of RF Circuits and System, Ministry of Education, Institute of Antennas and Microwave Technology, Hangzhou Dianzi University, Hangzhou 310018, China
[2]Smart City Research Center of Zhejiang Province, Hangzhou Dianzi University, Hangzhou 310018, China
[3]School of Electrical and Electronic Engineering, Nanyang Technological University, Singapore 639798

Corresponding author: Guo Qing Luo (luoguoqing@hdu.edu.cn)

ABSTRACT This paper presents a 3D band-absorptive frequency selective rasorber (FSR). Such an FSR is absorptive within a specific band and almost transparent below the absorption band. The definition and evaluation of the band-absorptive FSR is initially provided and followed by the design concept of 3D FSR. An example is then proposed, whose unit cell is composed of 3D absorber and 3D band-stop FSS. An equivalent circuit model is established for understanding its operating principle. A prototype of the proposed 3D band-absorptive FSR is fabricated. The measured results show that it has an absorption band ($|S_{11}| \leq -10$ dB and $|S_{21}| \leq -10$ dB) from 4.21 to 6.51 GHz, with a thickness of 0.17 wavelength at 4.21 GHz. Moreover, $|S_{21}|$ is higher than -1 dB at the frequencies below 1.28 GHz. The proposed band-absorptive FSR can be used as radomes for low-frequency antennas in military communications or spectrum monitoring systems.

INDEX TERMS Frequency selective rasorber (FSR), absorptive frequency selective structure, band-absorptive.

I. INTRODUCTIONN

Modern military platforms (aircrafts, ships, etc.) are receiving increasing attention for their stealthy performance. As a significant scattering source contributing to the overall radar cross section (RCS), antenna's RCS reduction is vital for a low-observable military platform. Among a variety of methods, utilizing frequency selective rasorbers (FSRs) [1] as stealthy radome is expected to have superior performance over conventionally used frequency selective surfaces/ structures (FSSs) [2]. An FSR should have a transmission window of low insertion loss (similar to a band-pass FSS), while it absorbs the out-of-band incident waves instead of reflecting them. Therefore, both monostatic and bistatic out-of-band RCS can be reduced.

An FSR can be seen as a combination of absorber and FSS. It is also termed as absorptive frequency selective structures (AFSS). The initial conceptual design, which is realized by cascading a lossy layer above a lossless two-dimensional (2-D) band-pass FSS layer, was introduced in an early patent [3]. A number of 2D designs were reported in the

subsequent publications [4]–[16]. Three-dimensional (3D) FSSs were also applied in the design of FSRs. By constructing absorption and transmission paths separately through lossless and lossy resonators in 3-D unit cells, several 3D FSRs were developed in [17]–[22]. Although the implementation of 3D structures is more complicated, 3D FSRs can easily achieve superior performance such as high selectivity (sharp roll-off of the pass-band) and stable filtering response under the oblique incidence.

The above mentioned FSRs have the following two features: one pass-band with limited bandwidth (usually less than 50% with $|S_{21}| \geq -3$ dB), and one or two absorption bands located at the lower or upper sides of the pass-band. Therefore, these FSRs are suitable for radomes of some radar antennas, whose operating bands are close or within the threatening bands of the incident EM waves, and their bandwidths are usually not very wide. However, there are a number of other applications like military communications and spectrum monitoring systems, whose antennas operate at frequencies below the typical threatening bands of the radar
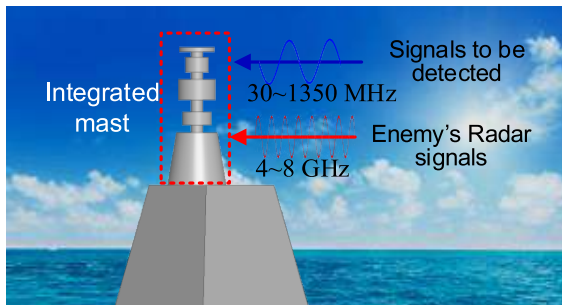
FIGURE 1. Sketch of a spectrum monitoring system.

systems, with bandwidths of several octaves. For example, a spectrum monitoring system covers 30 MHz to 1350 MHz, where several antennas or antenna arrays operating at different frequency bands are integrated around a mast, as seen in Fig. 1. It is obvious that the reported FSRs with a pass-band and one or two absorption bands are not suitable candidates for the stealthy radomes of these systems, because it is not possible to design a pass-band with an ultra-wide bandwidth at such low frequencies. Actually, such a stealthy radome can be realized by modifying the band-stop FSS by replacing its reflection band to an absorption band. Specifically, it has one or more absorption bands at the typical frequency bands of radars (e.g., C band or X band), and be almost transparent to the incident EM waves below the absorption bands. To be distinguished from the above mentioned FSRs in [4]–[22], FSRs that exhibit such characteristics are named as band-absorptive FSRs in this paper, while FSRs in [4]–[22] are named as band-pass FSRs.

Two previous designs with band-absorptive performance can be found in [23] and [24], which were designed to absorb 5.8 GHz wireless local area network signals and pass 900/1800/1900 MHz mobile-band signals. However, their absorption bandwidths (16% and 25.6%) are too narrow for radome applications. Some commercial absorbers without backing metallic surfaces [25], like polyurethane foam absorbers, exhibit similar performance as the band-absorptive FSR, even with an extremely wide absorption bandwidth. However, with the decrease of frequency, their transmission coefficients increase gradually, and a clear and sharp transition from absorption to transmission is not possible, at least for the current commercial absorbers.

In this paper, the definition and evaluation of the band-absorptive FSR is given for the first time. An FSR family can then be categorized into two types: band-pass and band-absorptive, similar to the classification of band-pass and band-stop FSSs. The concept and design of a 3D band-absorptive FSR is then proposed, whose unit-cell consists of two separate modes: absorption and transmission, which are realized by a 3D absorber and 3-D band-stop FSS, respectively. An equivalent circuit model is established and the operating principle is fully investigated. Its design guideline is also given. A prototype is then fabricated to verify the design, which exhibits an absorption bandwidth of 43%.
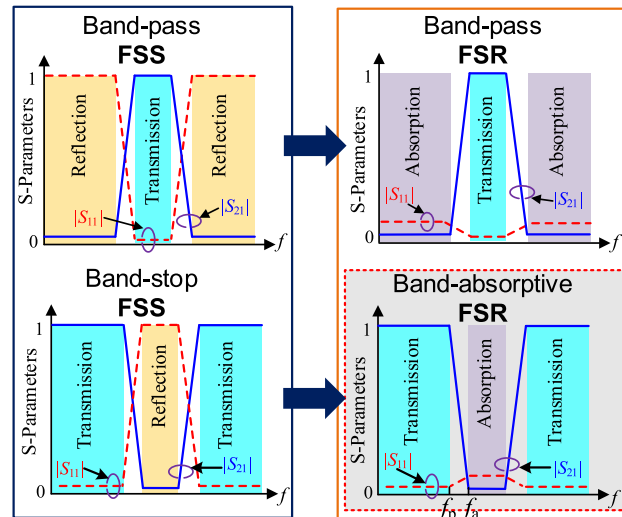

FIGURE 2. Reflection and transmission responses of an ideal band-pass FSS, band-pass FSR, band-stop FSS, and band-absorptive FSR.

Moreover, due to its small unit-cell size, stable filtering and absorption performance can be observed for the incident angle up to 30° in the *x-z* plane and 45° in the *y-z* plane.

II. CONCEPT

Fig. 2 illustrates the reflection and transmission coefficients ($|S_{11}|$ and $|S_{21}|$) of an ideal band-pass FSS, band-pass FSR, band-stop FSS, and band-absorptive FSR. It can be clearly seen that the previously reported band-pass FSR can be seen as a counterpart of a band-pass FSS, i.e., the reflection bands of the FSS are replaced by the absorption bands of FSR. Similarly, a band-absorptive FSR proposed in this paper can be seen as a counterpart of a band-stop FSS. It is realized by replacing the reflection band of a band-stop FSS by an absorption band.

The performance of a band-absorptive FSR can be evaluated by two factors: (i) the bandwidth of the absorption band, with both transmission and reflection coefficients less than −10 dB ($|S_{11}| \leq -10$ dB and $|S_{21}| \leq -10$ dB); (ii) the steepness of the transition from absorption to transmission, which can be evaluated as

$$FR_{ap} = f_a/f_p \qquad (1)$$

where f_a represents the starting frequency of the absorption band, and f_p represents the cut-off frequency of the transmission band. It is noted that f_p is defined as the highest frequency for the transmission coefficient higher than a specific value, e.g., −1 dB ($|S_{21}| \geq -1$ dB). It is well understood that an ideal band-absorptive FSR has FR_{ap} value close to 1, which means the absorption quickly transforms to transmission as the frequency decreases. Therefore, it can be used as a radome for an antenna whose highest frequency of the operating band is close to the absorption band of the FSR.

After describing the definition and evaluation of a band-absorptive FSR, a conceptual 3D design is depicted in Fig. 3,
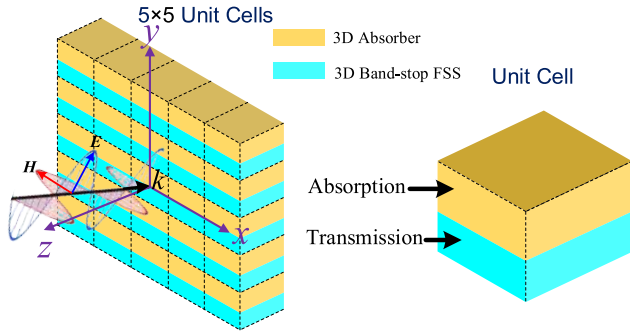
FIGURE 3. Illustration of a 3D band-absorptive FSR.

FIGURE 4. Generalized circuit models and *S*-parameters of a 3D absorber, a 3D band-stop FSS, and a 3D band-absorptive FSR.

which is composed of a 2-D periodic array of inner unit cells (5×5 unit cells are plotted in Fig. 3). Each unit cell is a two-mode cavity: one absorption mode and one transmission mode. The two modes are excited by the incident EM waves. To realize the above-mentioned band-absorptive characteristic, a possible solution of the two-mode cavity, as seen in Fig. 3, is a combination of a 3D absorber and 3D band-stop FSS, which are corresponding to the absorption and transmission paths, respectively.

To illustrate the feasibility of the proposed combination of the two-mode cavity in Fig. 3, we plot generalized circuit models and reflection/transmission coefficients of an ideal 3D absorber, 3D band-stop FSS and 3D band-absorptive FSR in Fig. 4. The key for the proposed band-absorptive FSR design is that the absorption band of the absorber and the reflection band of the band-stop FSS must overlap. In this case, the incident EM waves that cannot go through the band-stop FSS are absorbed by the absorber. Therefore, an absorption band of the band-absorptive FSR is obtained, with almost the same performance as the absorber. At frequencies below the absorption band, the absorber can hardly absorb the incident EM waves, thus most of them transmit through the band-stop FSS, which is naturally transparent. Hence, the proposed FSR has low-pass characteristic similar to the band-stop FSS.

We can further understand the operating principle of the band-absorptive FSR through some simple calculations of the impedance matrix. At f_a within the absorption band of the band-absorptive FSR, the ideal 3D band-stop FSS acts as a quasi-PEC block, and the incident EM waves cannot pass through it ($|S_{21}| = 0$). Therefore, its impedance matrix is

$$Z_{fss} = \begin{pmatrix} 0 & 0 \\ 0 & 0 \end{pmatrix} \quad (2)$$

As seen in Fig. 4 (c), the two sub-networks are connected in series. Hence, the impedance matrix of the band-absorptive FSR can be written as follows:

$$Z_{fsr} = Z_{absorber} + Z_{fss} = Z_{absorber} \quad (3)$$

which indicates that the band-absorptive FSR acts as the ideal absorber at f_a. Since all the incident EM waves are absorbed by the ideal absorber ($|S_{11}| = 0$ and $|S_{21}| = 0$), it can be
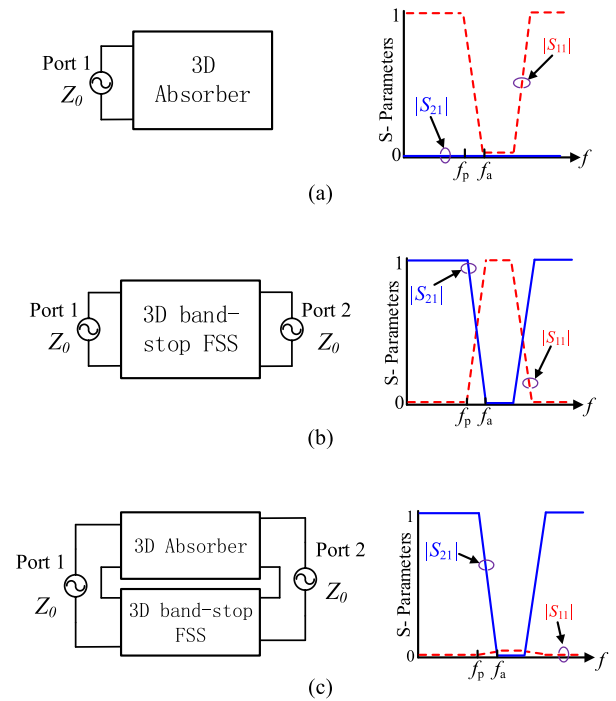
readily concluded that both reflection and transmission coefficients are zero at f_a for the band-absorptive FSR ($|S_{11}| = 0$ and $|S_{21}| = 0$).

At a lower frequency f_p, the ideal absorber acts as a quasi-PEC block, so its impedance matrix is

$$Z_{absorber} = \begin{pmatrix} 0 & 0 \\ 0 & 0 \end{pmatrix} \quad (4)$$

Therefore, the impedance matrix of the band-absorptive FSR at f_p can be written as follows:

$$Z_{fsr} = Z_{absorber} + Z_{fss} = Z_{fss} \quad (5)$$

III. DESCRIPTION OF THE PROPOSED 3D BAND-ABSORPTIVE FSR

Fig. 5 depicts the geometrical details of one unit-cell of the proposed 3D band-absorptive FSR. It is seen that each unit-cell consists of a 3D wideband absorber and a 3D band-stop FSS. The periods along the *x*- and *y*- directions are denoted by *W* and *H*, respectively. The 3D absorber is basically a shielded microstrip line which supports two quasi-TEM modes (air mode and substrate mode). When the incident EM waves along −*z* direction (normal incidence) strike the front surface of the absorber, they are coupled into the two transmission lines and finally absorber by the two resistors (R_a and R_s). An interdigital capacitor printed on the front substrate (substrate A_2) is used in series with the resistor R_a, instead of a chip capacitor in [26], which facilitates the fabrication and reduces the cost. The interdigital capacitor and chip resistor R_a are connected to the horizontal microstrip line and the
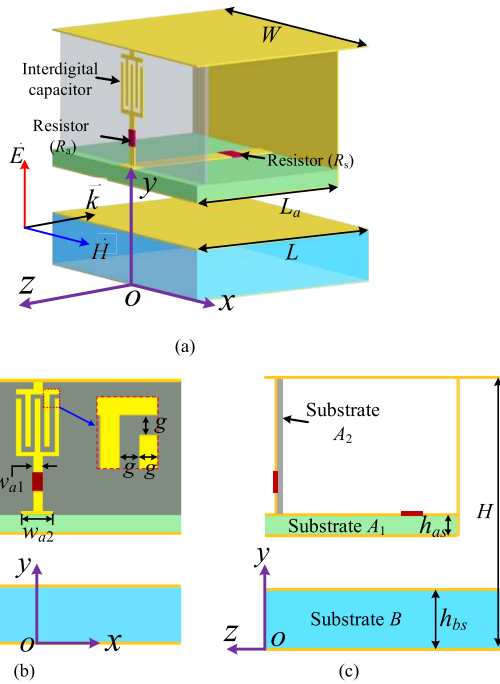
FIGURE 5. Geometry of one unit cell of the proposed band-absorptive FSR. (a) 3D view, (b) front view, and (c) side view. (Physical dimensions: $L = 12$ mm, $W = 15$ mm, $H = 16.8$ mm, $L_a = 9.8$ mm, $h_a = 8$ mm, $h_{as} = 1.016$ mm, $w_{a1} = 0.5$ mm, $w_{a2} = 1.5$ mm, $g = 0.25$ mm, $h_b = 8.8$ mm, and $h_{bs} = 4.064$ mm).

upper copper sheet by copper lines with a width of w_{a1}. The microstrip line is printed on substrate A_1, with another resistor R_s inserted near its back end. Both resistors are with the same resistance of 250 Ω. The relative permittivity of substrate A_1 and A_2 are 2.2, and their thicknesses are 1.016 mm and 0.508 mm, respectively.

The unit cell of the band-stop FSS is a stacked structure of two parallel-plate waveguides (PPWs): one is filled with air and the other with substrate B, whose relative permittivity is 10.2 and thickness is 4 mm. The two PPWs can be seen as two transmission lines (TLs) in series, with different characteristic impedance and electric lengths. With proper parameters, two transmission poles can be achieved leading to a wide reflection band.

IV. OPERATING PRINCIPLE

An equivalent circuit model of the proposed band-absorptive FSR is established to help understand the operating principle, as seen in Fig. 6. This model can be divided into two series sub-networks, which represent the 3D absorber and band-stop FSS, respectively. For the absorber, the two transmission lines (Z_{a1}, θ_{a1}) and (Z_{a2}, θ_{a2}) represent the air and substrate microstrip lines, respectively, each of which corresponds to one quasi-TEM mode. Their characteristic impedances and electric lengths are extracted from the Eigen-mode Solver of CST [27]. The series *RLC* circuit (R_a, L_a and C_a) that connects the front end of the air TL represents the resistor, interdigital capacitor, and the strip on the front substrate.
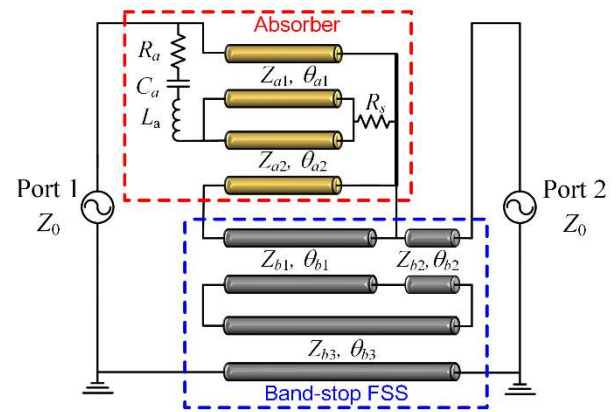
FIGURE 6. Equivalent circuit model of the proposed band-absorptive FSR. (Circuit parameters: $Z_0 = 422$ Ω, $Z_{a1} = 132$ Ω, $Z_{a2} = 34$ Ω, $Z_{b1} = 119$ Ω, $Z_{b2} = 320$ Ω, $Z_{b3} = 32$ Ω, $R_a = R_s = 250$ Ω, $L_a = 1.7$ nH, $C_a = 0.3$ pF, $\theta_{a1} = 180°$ at 15.3 GHz, $\theta_{a2} = 180°$ at 7.7 GHz, $\theta_{b1} = 180°$ at 15.3 GHz, $\theta_{b2} = 180°$ at 68.2 GHz, and $\theta_{b3} = 180°$ at 3.9 GHz).

Another resistor (R_s) at the end of the TLs is shared by both air and substrate TLs. It is seen that the substrate mode is absorbed by R_s while the air mode is absorbed by both R_s and R_a. Moreover, C_a can also be tuned to ensure a good impedance match. Therefore, most of the incident waves are expected to couple into the air-mode TL. To realize this, the height of the air microstrip line (h_a-h_{as}) is chosen to be much higher than that of the substrate microstrip line (h_{as}).

For the band-stop FSS, the circuit is simply a combination of two transmission lines in series, which represent the two PPWs filled with air and substrate B. It is noted that the air transmission line is with two sections. The short section (Z_{b2}, θ_{b2}) represents the end part of the PPW with height of (H-h_{bs}) and length of (L-L_a). Their characteristic impedances and electric lengths can be calculated by

$$Z_{b1} = \eta_0(h_b - h_{bs})/W \qquad (6a)$$

$$Z_{b2} = \eta_0(H - h_{bs})/W \qquad (6b)$$

$$Z_{b3} = \eta_0 h_{bs}/(W\sqrt{\varepsilon_r}) \qquad (6c)$$

$$\theta_{b1} = 2\pi f L_a/c_0 \qquad (7a)$$

$$\theta_{b2} = 2\pi f(L - L_a)/c_0 \qquad (7b)$$

$$\theta_{b3} = 2\pi f L\sqrt{\varepsilon_r}/c_0 \qquad (7c)$$

where $\eta_0 = 377$ Ω, c_0 is the speed of light in free-space and f is the operating frequency.

The reflection band of the band-stop FSS can be determined by the first two transmission zeros, which can be calculated by
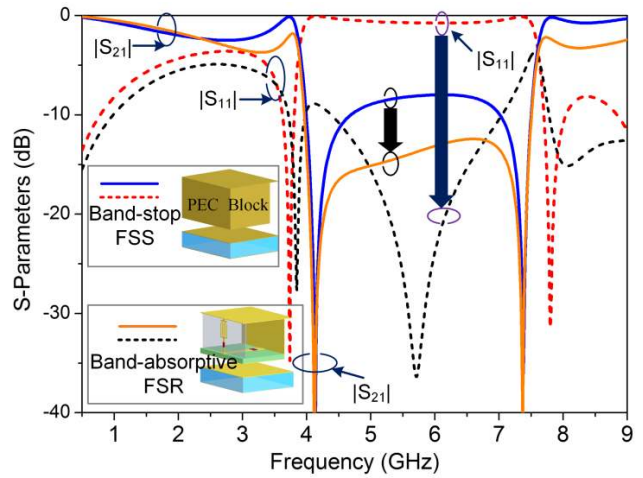
$$\sin(\theta_{b3}/\sqrt{\varepsilon_r}) + \sqrt{\varepsilon_r}(h_b - h_{bs})/h_{bs}\sin\theta_{b3} \qquad (8)$$

It is noted that (8) can be obtained by writing the *S*-matrix of a typical 3D band-stop FSS consisting of two stacked PPWs and solving $|S_{21}| = 0$.
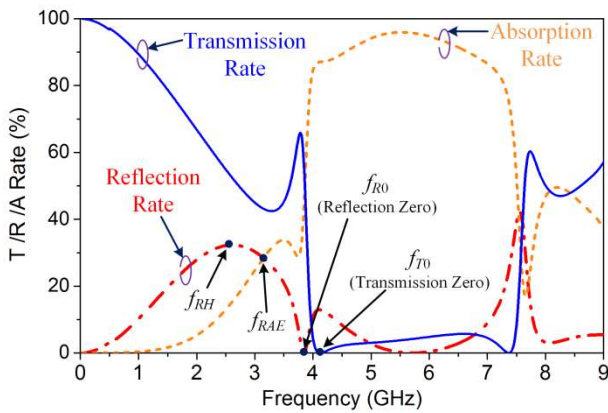
Fig. 7 plots the *S*-parameters from 30 MHz to 9 GHz of the proposed band-absorptive FSR, calculated from Advanced
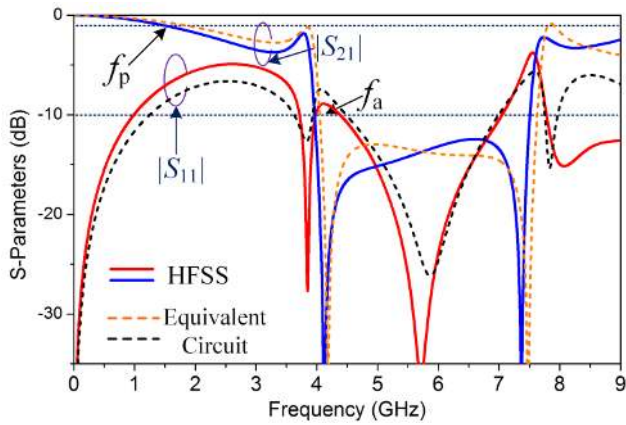
FIGURE 7. Comparison of the *S*-parameters of the proposed band-absorptive FSR under the normal incidence obtained from full-wave simulation (HFSS) and the equivalent circuit model (ADS).

FIGURE 8. Simulated transmission, reflection and absorption rates of the proposed band-absorptive FSR.

FIGURE 9. Comparison of the *S*-parameters of the proposed band-absorptive FSR and the band-stop FSS.

Design System (ADS) and simulated using High Frequency Structure Simulator (HFSS). A good agreement of these results can be observed. It is seen from the simulated results in Fig. 6 that the proposed band-absorptive FSR has an absorption band ($|S_{11}| \leq -10$ dB and $|S_{21}| \leq -10$ dB) from 4.38 GHz (f_a) to 7.05 GHz, corresponding to a 46.7% fractional bandwidth at the center frequency of 5.715 GHz. Below the absorption band, $|S_{21}|$ gradually increases as the frequency decreases. It is seen that $|S_{21}|$ is above -1 dB when the frequency is below 1.47 GHz (f_p). Therefore $FR_{ap} = 3.0$ can be readily calculated using (1). It is obvious that decreasing FR_{ap} is an important issue of our future work. It is also worth mentioning that $|S_{21}|$ increases to -0.5 dB at 1.02 GHz and -0.1 dB at 415 MHz, which indicate very low insertion loss at low frequencies.

In order to demonstrate which factors affect FR_{ap}, we plot the transmission rate ($|S_{21}|^2$), reflection rate ($|S_{11}|^2$), and absorption rate ($1 - |S_{11}|^2 - |S_{21}|^2$) in Fig. 8. It is clear that in the absorption band, both the reflection and transmission rates are small, while the absorption rate is around 90%. When the frequency decreases from f_{T0} (transmission-zero frequency)

to f_{R0} (reflection-zero frequency), the absorption rate drops off while the transmission rate increases severely. Below f_{R0}, it is seen that the absorption rate slightly arises, and then goes down continuously with the decrease of frequency. However, the reflection rate rises up to 32% as the frequency decreases from f_{R0} to f_{RH} (the highest-reflection frequency below f_{R0}), and then moves downward as the frequency decreases from f_{RH}. It is clear to see that the reflection rate is higher than the absorption rate below the frequency of f_{RAE}, which means the reflection contributes more to the insertion loss than the absorption. For example, at 1 GHz, the absorption rate is only 0.37%, which can be neglected.

In Fig. 9, we plot the transmission and reflection coefficients of the proposed band-absorptive FSR and the band-stop FSS which is one part of it, in order to illustrate the relationship between them. It is noted that the simulation model of the band-stop FSS is realized by simply replacing the absorber with a PEC block in the band-absorptive FSR, as seen in the inset of Fig. 9. It is seen that at low frequencies (below the absorption band of the band-absorptive FSR), both $|S_{11}|$ and $|S_{21}|$ of the band-absorptive FSR are very similar to those of the band-stop FSS, which verifies our analysis in Section II (see (5)). It is also seen that the two transmission poles of the band-absorptive FSR strictly match that of the band-stop FSS, which proves that the absorption band of the band-absorptive FSR is determined by the reflection band of the band-stop FSS. With the help of the absorber that absorbs the incident EM waves within the absorption band, both $|S_{11}|$ and $|S_{21}|$ of the band-absorptive FSR is lowered compared with the band-stop FSS, as seen in Fig. 9.

As we have mentioned, the reflection contributes more to the insertion loss at low frequencies of the band-absorptive FSR, compared with the absorption. Fig. 9 further illustrates that the reflection is relevant to the band-stop FSS. It is noted that the high reflection rate below the reflection-zero frequency is common for the broadband band-stop FSS. If the

reflection band is narrower, the reflection rate can be lower, thus the insertion loss of the band-absorptive FSR can be smaller, leading to a smaller FR_{ap} value. It is a tradeoff between the FR_{ap} value and the bandwidth of the absorption band, at least for the proposed design. Future work will focus on both the expansion of the absorption band and the reduction of FR_{ap} value.

After understanding the operating principle of the proposed band-absorptive FSR, a design guideline can be formulated as follows.

(1) As mentioned earlier, the absorption band of the FSR approximately overlaps with the reflection band of the band-stop FSS. Therefore, the physical dimensions of the 3D band-stop FSS should be chosen to ensure a certain reflection band. Due to the bandwidth requirements, two transmission zeros are needed. Hence, a higher relative permittivity of substrate B, e.g., 10.2, is preferred. The height ratio h_{bs}/h_b can be initially set to 0.5. An initial thickness L can be chosen to obtain the desired two transmission zeros according to (8).

(2) The center frequency of the 3D absorber (f_{ca}) is approximately around $f_{ca} = c / (2L_a + H_a)$. A lower relative permittivity of substrate A_1 is preferred. The height ratio h_{as}/h_a can be initially set to 1/8.

(3) Simulations of the 3D absorber and the band-stop FSS can be conducted separately based on the initial parameters. A small adjustment of these parameters can be made to roughly obtain the absorption band of the absorber and the reflection band of the band-stop FSS.

(4) A final simulation of the proposed FSR combining the band-stop FSS and absorber is conducted. The structure parameter may be fine-tuned for optimum performance.

V. EXPERIMENTAL VERIFICATION

A prototype of the proposed band-absorptive FSR is fabricated and measured in order to verify our design. The prototype consists of 12 unit cells along the x-direction, with a size of 180 mm × 16.8 mm × 12 mm, as seen in Fig. 10 (a). Rogers RT5880 and RT6010 are used for substrate A and B, respectively. The resistors used are Vishay CH0402- 250RGFPT. The air separation between substrates A_1 and B is supported by three Teflon rods with diameters of 4 mm.

A parallel-plate waveguide setup is used for our measurement, as seen in Fig. 10 (b), whose details were described in [28]. It is mentioned that its upper plate is removed in the figure for a better view. The height of the PPW (16.8 mm) is equal to the height of the fabricated prototype, which allows a dominant TEM mode travelling inside the PPW. To avoid reflections from the four edges of the PPW, they are covered with commercial polyurethane foam absorber. Two cones are located at the ends of the PPW in order to achieve a good transition from the coaxial line to the PPW.

Fig. 10 (c) shows the comparison of simulated and measured transmission and reflection coefficients under the normal incidence, which exhibits a relatively good agreement. The measured $|S_{11}|$ shows a higher value than the simulated
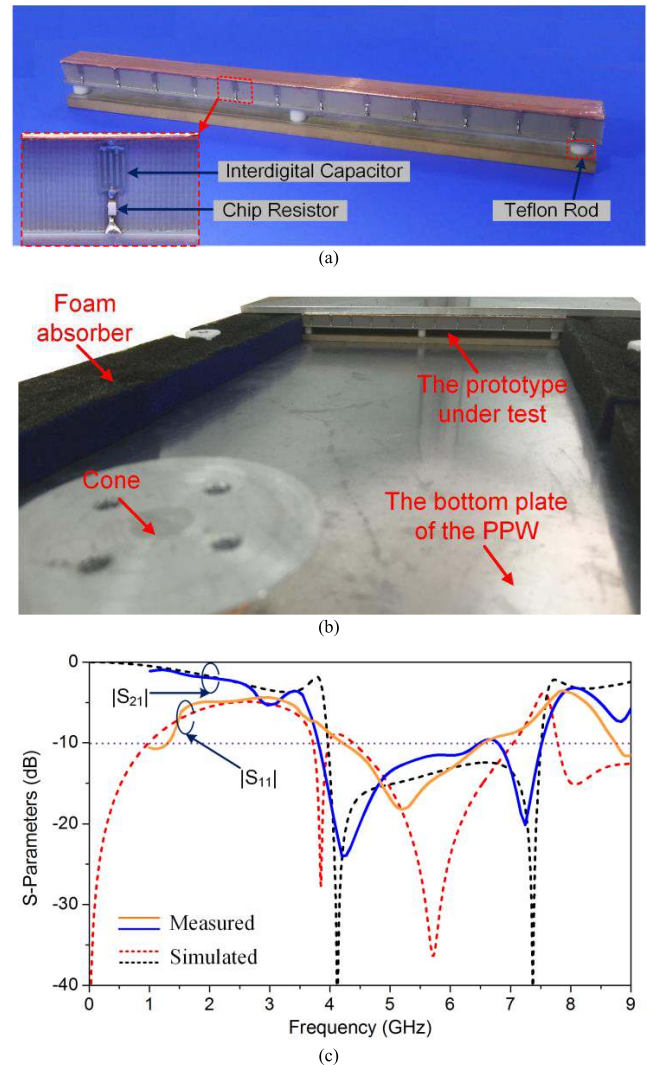
FIGURE 10. (a) Fabricated prototype of the proposed band-absorptive FSR, (b) the prototype in a PPW measurement set-up, and (c) measured and simulated S-parameters of the prototype under the normal incidence.

one above 5.2 GHz and a frequency shift is also observed, which leads to a slightly narrower absorption bandwidth compared to the simulated results. The difference may be due to the assembly error of the prototype, the parasitic effects of the lumped resistors, and the measurement error from the PPW setup (the foam absorbers are not perfect to prevent the reflected waves). The measured absorption band ($|S_{11}| \leq -10$ dB and $|S_{21}| \leq -10$ dB) is from 4.21 GHz (f_a) to 6.51 GHz, corresponding to a 43% fractional bandwidth (FBW) at the center frequency of 5.36 GHz, which is a little narrower and lower than the simulated bandwidth (46.7%, 5.715 GHz). Moreover, the thickness of the proposed band-absorptive FSR is $0.17\lambda_a$, where λ_a is the free-space wavelength at f_a (the starting frequency of the absorption band).

At lower frequencies, $|S_{21}|$ gradually increases as the frequency decreases, the cut-off frequency for $|S_{21}| = -1$ dB is 1.28 GHz (f_p), which is also a little lower than the simulated one. The frequency ratio FR_{ap} for the measured
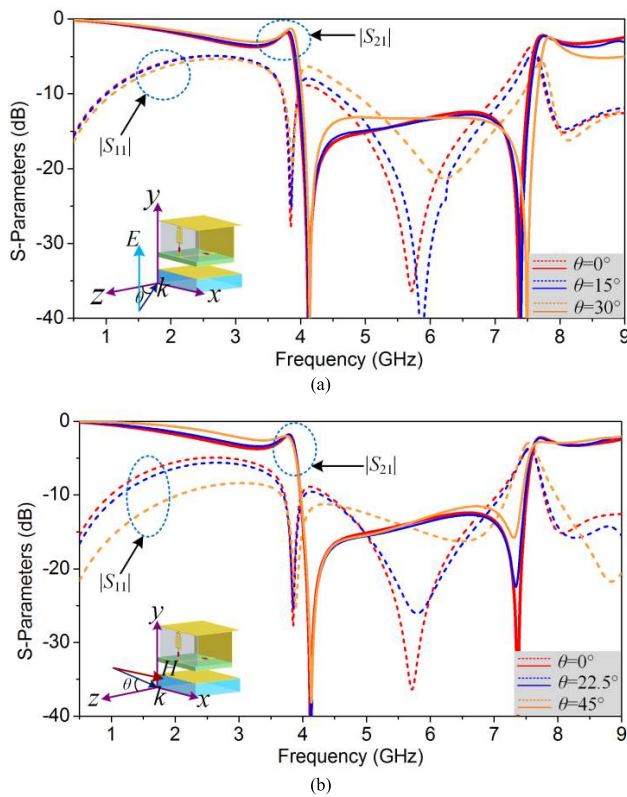
FIGURE 11. Simulated *S*-parameters of the proposed band-absorptive FSR under the oblique incidence in (a) *x-z* (0°, θ) and (b) *y-z* (90°, θ) planes.

result is then calculated to be 3.3, which is a little bit larger than the simulated one (3.0). It is noted that the lowest operating frequency of the parallel-plate waveguide setup is 1 GHz, which limits our lowest measured frequency at 1 GHz.

The simulated transmission and reflection coefficients under the oblique incidence scanned in the *x-z* and *y-z* planes are plotted in Figs. 11 (a) and (b), respectively, which exhibit stable frequency responses (especially in the *y-z* plane). Specifically, when the incident angle in the *y-z* plane increases, the absorption band expands, and the reflection level at low frequencies reduces, which results in a lower transmission loss. It is seen in Fig. 11 (b) that for θ = 45°, the FBW of the absorption band is 58.0%, and FR_{ap} = 1.76, indicating a much better performance compared with that under the normal incidence (θ = 0°). It is worth noting that the stability under the oblique incidence in the *y-z* plane is better than that in the *x-z* plane, as seen in Fig. 11. This is well understood because for each PPW section, the height (h_{bs}, etc.) along the *y*-direction is much smaller than the width in the *x*-direction (*W*). It is noted that only the measurement under the normal incidence can be implemented using the measurement setup in Fig. 10(b), therefore simulated performances under the oblique incidence are provided.

Finally, comparisons are made with the 2-D band-absorptive FSR in [23] and [24]. Although the proposed 3-D

structure has a little bit larger FR_{ap} value than that in [23], it has a smaller unit-cell size than that of both designs in [18] and [24], which results in superior performance under the oblique incidence. Moreover, the proposed 3D design exhibits much wider absorption bandwidth, which is 2.7 times of that in [23] and 1.8 times of that in [24].

VI. CONCLUSION
This paper has presented a 3D band-absorptive FSR. The design concept has been introduced, the geometry of its implementation has been described, and its operating principle has been explained along with simulated and measured results. The unit cell of the proposed design, which is a combination of a 3D absorber and a 3D band-stop FSS, exhibits an absorption band at high frequencies and is almost transparent at low frequencies. The measured absorption band ($|S_{11}| \leq -10$ dB and $|S_{21}| \leq -10$ dB) is from 4.21 GHz to 6.51 GHz, while $|S_{21}|$ is higher than −1 dB at the frequencies below 1.28 GHz. The proposed design also exhibits stable angular response under the oblique incidence. The proposed band-absorptive FSR has potential applications in low-RCS radomes for low-frequency antennas. Further improvements include expansion of the absorption band, reduction of FR_{ap} value, and curved structures for practical radomes.

REFERENCES
[1] B. A. Munk, *Metamaterials: Critique and Alternatives*. Hoboken, NJ, USA: Wiley, 2009.
[2] B. A. Munk, *Frequency Selective Surfaces: Theory and Design*. New York, NY, USA: Wiley, 2000.
[3] W. S. Arceneaux, R. D. Akins, and W. B. May, "Absorptive/transmissive radome," U. S. Patent 5 400 043 A, Mar. 21, 1995.
[4] F. Costa and A. Monorchio, "A frequency selective radome with wideband absorbing properties," *IEEE Trans. Antennas Propag.*, vol. 60, no. 6, pp. 2740–2747, Jun. 2012.
[5] A. Motevasselian and B. L. G. Jonsson, "Design of a wideband rasorber with a polarisationsensitive transparent window," *IET Microw., Antennas Propag.*, vol. 6, no. 7, pp. 747–755, May 2102.
[6] Y. Shang, Z. Shen, and S. Xiao, "Frequency-selective rasorber based on square-loop and cross-dipole arrays," *IEEE Trans. Antennas Propag.*, vol. 62, no. 11, pp. 5581–5589, Nov. 2014.
[7] H. Zhou *et al.*, "Experimental demonstration of an absorptive/ transmissive FSS with magnetic material," *IEEE Antennas Wireless Propag. Lett.*, vol. 13, pp. 114–117, 2014.
[8] Q. Chen, J. Bai, L. Chen, and Y. Fu, "A miniaturized absorptive frequency selective surface," *IEEE Antennas Wireless Propag. Lett.*, vol. 15, pp. 80–83, 2015.
[9] Q. Chen, S. Yang, J. Bai, and Y. Fu, "Design of absorptive/transmissive frequency-selective surface based on parallel resonance," *IEEE Trans. Antennas Propag.*, vol. 65, no. 9, pp. 4897–4902, Sep. 2017.
[10] H. Huang and Z. Shen, "Absorptive frequency-selective transmission structure with square-loop hybrid resonator," *IEEE Antennas Wireless Propag. Lett.*, vol. 16, pp. 3212–3215, 2017.
[11] K. Zhang, W. Jiang, and S. Gong, "Design bandpass frequency selective surface absorber using LC resonators," *IEEE Antennas Wireless Propag. Lett.*, vol. 16, pp. 2586–2589, 2017.
[12] Y. Han, W. Che, X. Xiu, W. Yang, and C. Christopoulos, "Switchable low-profile broadband frequency-selective rasorber/absorber based on slot arrays," *IEEE Trans. Antennas Propag.*, vol. 65, no. 12, pp. 6998–7008, Dec. 2017.
[13] S. Zhong, L. Wu, T. Liu, J. Huang, W. Jiang, and Y. Ma, "Transparent transmission-selective radar-infrared bi-stealth structure," *Opt. Express*, vol. 26, no. 13, pp. 16466–16476, Jun. 2018.
[14] Z. Wang *et al.*, "A high-transmittance frequency-selective rasorber based on dipole arrays," *IEEE Access*, vol. 6, pp. 31367–31374, 2018.

[15] X. Xiu, W. Che, Y. Han, and W. Yang, "Low-profile dual-polarization frequency-selective rasorbers based on simple-structure lossy cross-frame elements," *IEEE Antennas Wireless Propag. Lett.*, vol. 17, no. 6, pp. 1002–1005, Jun. 2018.

[16] Q. Chen, D. Sang, M. Guo, and Y. Fu, "Frequency-selective rasorber with interabsorption band transparent window and interdigital resonator," *IEEE Trans. Antennas Propag.*, vol. 66, no. 8, pp. 4105–4114, Aug. 2018.

[17] B. Li and Z. Shen, "Wideband 3D frequency selective rasorber," *IEEE Trans. Antennas Propag.*, vol. 62, no. 12, pp. 6536–6541, Dec. 2014.

[18] Z. Shen, J. Wang, and B. Li, "3-D frequency selective rasorber: Concept, analysis, and design," *IEEE Trans. Microw. Theory Techn.*, vol. 64, no. 10, pp. 3087–3096, Oct. 2016.

[19] Y. Yu, Z. Shen, T. Deng, and G. Luo, "3-D frequency-selective rasorber with wide upper absorption band," *IEEE Trans. Antennas Propag.*, vol. 65, no. 8, pp. 4363–4367, Aug. 2017.

[20] T. Deng, Y. Yu, and Z. Chen, "A broadband 3D frequency selective rasorber by using magnetic materials," in *Proc. Int. Conf. Electromagn. Adv. Appl. (ICEAA)*, Verona, Italy, Sep. 2017, pp. 1731–1734.

[21] A. A. Omar, Z. Shen, and H. Huang, "Absorptive frequency-selective reflection and transmission structures," *IEEE Trans. Antennas Propag.*, vol. 65, no. 11, pp. 6173–6178, Nov. 2017.

[22] Y. Zhang, B. Li, L. Zhu, Y. Tang, Y. Chang, and Y. Bo, "Frequency selective rasorber with low insertion loss and dual-band absorptions using planar slotline structures," *IEEE Antennas Wireless Propag. Lett.*, vol. 17, no. 4, pp. 633–636, Apr. 2018.

[23] G. I. Kiani, A. R. Weily, and K. P. Esselle, "A novel absorb/transmit FSS for secure indoor wireless networks with reduced multipath fading," *IEEE Microw. Wireless Compon. Lett.*, vol. 16, no. 6, pp. 378–380, Jun. 2006.

[24] G. I. Kiani, K. L. Ford, K. P. Esselle, A. R. Weily, and C. J. Panagamuwa, "Oblique incidence performance of a novel frequency selective surface absorber," *IEEE Trans. Antennas Propag.*, vol. 55, no. 10, pp. 2931–2934, Oct. 2007.

[25] *ECCOSORB LS Foamabsorbers*, Emerson & Cuming Microw. Products, Randolph, MA, USA, 2018. [Online]. Available: http://www.eccosorb.com/products-eccosorb-ls.htm

[26] A. K. Rashid, Z. Shen, and S. Aditya, "Wideband microwave absorber based on a two-dimensional periodic array of microstrip lines," *IEEE Trans. Antennas Propag.*, vol. 58, no. 12, pp. 3913–3922, Dec. 2010.

[27] A. A. Omar and Z. Shen, "Double-sided parallel-strip line resonator for dual-polarized 3-D frequency-selective structure and absorber," *IEEE Trans. Microw. Theory Techn.*, vol. 65, no. 10, pp. 3744–3752, Oct. 2017.

[28] Y. Shang, Z. Shen, and S. Xiao, "On the design of single-layer circuit analog absorber using double-square-loop array," *IEEE Trans. Antennas Propag.*, vol. 61, no. 12, pp. 6022–6029, Dec. 2013.

GUO QING LUO (M'08) received the B.S. degree from the China University of Geosciences, Wuhan, China, in 2000, the M.S. degree from Northwest Polytechnical University, Xi'an, China, in 2003, and the Ph.D. degree from Southeast University, Nanjing, China, in 2007.

Since 2007, he has been a Lecturer with the Faculty of School of Electronics and Information, Hangzhou Dianzi University, Hangzhou, China, and was promoted to Professor, in 2011. From 2013 to 2014, he was with the Department of Electrical, Electronic and Computer Engineering, Heriot-Watt University, Edinburgh, U.K., as a Research Associate, where he was involved in developing low profile antennas for UAV applications. He has authored or co-authored over 80 technical papers in refereed journals and conferences, and he holds 16 patents. His current research interests include RF, microwave and mm-wave passive devices, antennas, and frequency selective surfaces.

Dr. Luo is a member of the IEEE AP-Society and the MTT-Society. He was a recipient of the CST University Publication Award, in 2007, the National Excellent Doctoral Dissertation of China, in 2009, and the National Natural Science Award (the second class) of China, in 2016. He served as the TPC Chair of the 2018 U.K.-Europe-China Workshop on Millimetre-Waves and Terahertz Technologies (UCMMT2018) and the 2017 National Conference on Microwave and Millimeter Waves (NCMMW2017) and as the Organizing Committee Chair of the 2011 China-Japan Joint Microwave Conference (CJMW2011). He also serves as a Reviewer for many technical journals, including the IEEE TRANSACTIONS ON ANTENNAS AND PROPAGATION, IEEE TRANSACTIONS ON MICROWAVE THEORY AND TECHNIQUES, IEEE ANTENNAS AND WIRELESS PROPAGATION LETTERS, and IEEE MICROWAVE AND WIRELESS COMPONENTS LETTERS.

QI LIU received the B.E. degree in optical engineering and the Ph.D. degree in optical communication technology from Zhejiang University, Hangzhou, China, in 2011 and 2016, respectively.

From 2014 to 2015, she was a joint Ph.D. student with the School of Electrical and Computer Engineering, Georgia Institute of Technology. From 2016 to 2017, she was with the Research Institute of China Electronics Technology Group Corporation, where she has been an Engineer, since 2016. In 2017, she joined Hangzhou Dianzi University, where she is currently a Research Assistant Professor. Her current research interests include wideband antenna arrays, RFID antennas and sensors, and wearable and printed electronics.

YUFENG YU received the B.S. degree from the University of Electronic Science and Technology of China, Chengdu, China, in 2008, and the Ph.D. degree from Zhejiang University, Hangzhou, China, in 2013.

From 2013 to 2017, he was with the Research Institute of China Electronics Technology Group Corporation, where he has been a Senior Engineer, since 2015. In 2016, he spent seven months with Temasek Laboratories, National University of Singapore, as a Research Scientist. Since 2017, he has been with the School of Electronics and Information, Hangzhou Dianzi University, Hangzhou.

He has authored or co-authored over 30 technical papers in refereed journals and conferences, and he holds three patents. His current research interests include frequency selective surfaces/structures and antennas.

WEILIANG YU received the B.S. degree in electronic information engineering from Hangzhou Dianzi University, Hangzhou, China, in 2016, where he is currently pursuing the Ph.D. degree in electromagnetic field and microwave technology. His current research interests include frequency selective structures and microwave absorbers.

HUAYAN JIN was born in Hangzhou, Zhejiang, China, in 1989. She received the B.S. degree in electronic engineering and Ph.D. degree in electromagnetic field and microwave technology from the Nanjing University of Science and Technology, Nanjing, China, in 2011 and 2017, respectively. From August 2012 to January 2013, May 2013 to October 2013, and April 2014 to October 2014, she was an exchange student with Chang Gung University, Taoyuan, Taiwan.

She is currently a Lecturer with the School of Electronics and Information, Hangzhou Dianzi University, Hangzhou. Her main research interests include millimeter-wave antennas, differential-fed antennas, and filtering antennas. She serves as a Reviewer for the IEEE Access, *IET Electronics Letters*, and the *International Journal of Electronics*.

ZHEN LIAO received the B.S. degree from Nanchang Hangkong University, Nanchang, China, in 2009, the M.S. degree from the Nanjing University of Science and Technology, Nanjing, China, in 2012, and the Ph.D. degree from Southeast University, Nanjing, in 2017. He is currently a Lecturer with the School of Electronics and Information, Hangzhou Dianzi University, Hangzhou, China. His current research interests include microwave plasmonics, antennas, and metamaterials.

ZHONGXIANG SHEN (M'98–SM'04–F'17) received the B.Eng. degree from the University of Electronic Science and Technology of China, Chengdu, China, in 1987, the M.S. degree from Southeast University, Nanjing, China, in 1990, and the Ph.D. degree from the University of Waterloo, Waterloo, ON, Canada, in 1997, all in electrical engineering.

From 1990 to 1994, he was with the Nanjing University of Aeronautics and Astronautics, China. He was with Com Dev Ltd., Cambridge, Canada, as an Advanced Member of Technical Staff, in 1997. He spent six months each, in 1998, first with the Gordon McKay Laboratory, Harvard University, Cambridge, MA, USA, and then with the Radiation Laboratory, University of Michigan, Ann Arbor, MI, USA, as a Postdoctoral Fellow. In 1999, he joined Nanyang Technological University, Singapore, as an Assistant Professor, where he is currently a Full Professor. He served as the Chair for the IEEE MTT/AP Singapore Chapter, in 2009. He was the Chair of the IEEE AP-S Chapter Activities Committee, from 2010 to 2014. He is currently the Secretary of the IEEE AP-S. He is currently an Associate Editor of the IEEE Transactions on Antennas and Propagation.

He has authored or co-authored more than 170 journal papers (among them 100 were published in IEEE journals) and has presented more than 160 conference papers. His research interests include design of small and planar antennas for various wireless communication systems, analysis and design of frequency-selective structures, and hybrid numerical techniques for modeling RF/microwave components and antennas.

. . .